PAPER

Check for updates

A study on interfacial structure design and thermal conductivity optimization of diamond/copper composites

Dandan Li, [ID] [ac] Jian Wang, [bc] Yunzhen Jiang, [d] Zhanghui Liu, [c] Guojie Huang,*[b] Jinsong Feng, [a] Bo Peng, [a] Bing Wang [a] and Ruzhi Wang [ID] *[a]

Diamond/copper composites have garnered significant interest due to their high thermal conductivity, playing a crucial role in next-generation high-density integrated electronic components. Currently, enhancing the interfacial bonding strength between diamond and the copper matrix through intermediate layers to improve composite thermal conductivity constitutes a major research focus in this field. However, the diamond/copper interfacial structure and its high thermal conductivity mechanisms remain unclear. To address this, this study employed first-principles calculations to investigate three interfacial structures: copper/zirconium carbide (Cu/ZrC), copper/titanium carbide (Cu/TiC), and copper/tungsten carbide (Cu/WC). Among these, the Cu/TiC interface was identified as having stronger binding ability for combining the copper matrix with diamond than Cu/ZrC and Cu/WC. Subsequently, the thermal conductivity performance of diamond/copper composites with the TiC interfacial layer was investigated using the finite element analysis (FEA) and the interfacial thermal resistance theory. This study systematically explored the effects of the diamond volume fraction, particle size, and interfacial layer thickness on the thermal conductivity and coefficient of thermal expansion of the composites. The results demonstrate that our computational findings closely match experimentally measured values: at diamond particle sizes of 100 μm and 230 μm, the simulated thermal conductivities of 664 W m^{-1} K^{-1} and 763 W m^{-1} K^{-1} align with experimental measurements of 654 W m^{-1} K^{-1} and 752 W m^{-1} K^{-1}, respectively. Furthermore, the observed trends consistently correspond to experimental data, confirming that both thermal conductivity and the coefficient of thermal expansion decrease with the increasing interfacial layer thickness. And thermal conductivity and the coefficient of thermal expansion increase with increasing diamond particle size. Conversely, thermal conductivity increases when the coefficient of thermal expansion decreases with increasing diamond volume fraction. Our simulation results demonstrate excellent agreement with published experimental data and established trends. This study presents simulation approaches and fitting formulas for the thermal conductivity and coefficient of thermal expansion, providing theoretical guidance for the design, fabrication, and application of diamond/copper-based composite thermal management materials.

1. Introduction

With the rapid development of fifth-generation mobile communications (5G), high-power lasers, and third-generation semiconductor devices, the power density of electronic equipment has grown exponentially. Traditional packaging materials (*e.g.*, Al/SiC and W/Cu) cannot meet the dual demands of extreme heat dissipation (>1000 W cm^{-2}) and low thermal expansion coefficient matching (CTE $\leq 5 \times 10^{-6}$/K). Relevant studies indicate that for every 18 °C increase in the operating temperature of semiconductor components, the failure rate increases by 2–3 times.[1,2] Consequently, thermal management is as critical as performance for semiconductor devices. Against this backdrop, diamond/copper composites have emerged as a research hotspot for high-thermal-conductivity electronic packaging materials, leveraging the synergistic effect of diamond's ultrahigh intrinsic thermal conductivity (>2000 W m^{-1} K^{-1})[3] and the copper matrix's excellent processability. However, poor interfacial wettability between

[a] *State Key Laboratory of Materials Low-Carbon Recycling, College of Materials Science and Engineering, Beijing University of Technology, Beijing, 100124, China. E-mail: wrz@bjut.edu.cn*

[b] *China Nonferrous Metal Mining (Group) Co., Ltd., Beijing, 100029, China. E-mail: huangguojiepaper@126.com*

[c] *China Nonferrous Metals Innovation Institute (Tianjin) Co., Ltd., Tianjin, 300393, China*

[d] *Guilin Tebon Superhard Material Co., Ltd, Guilin, 541994, China*

diamond and copper results in high interfacial thermal resistance, limiting their practical application. Therefore, selecting suitable interfacial layers for diamond/copper composites remains a key research focus.

Current studies on interfacial layers in diamond/copper composites primarily rely on experimental methods. Chen et al.[4] demonstrated that a Ti content of 0.6 wt% leads to the formation of a continuous 400 nm TiC layer in composites containing 120 μm diamond at 50 vol%, thereby yielding a peak thermal conductivity of 704 W m^{-1} K^{-1}. Wu et al.[5] prepared diamond/copper composites via vacuum hot-pressing sintering and investigated the effect of Ti on thermal conductivity. Zhang et al.[6] designed a bilayer structure on diamond particles and used vacuum hot-pressing sintering to fabricate dense diamond/copper composites with superior thermal performance. Chung et al.[7] studied the thermal properties of diamond/Cu–Ti composites sintered at 1373 K for 30 min using pressureless melt infiltration. Wang et al.[8] employed spark plasma sintering to prepare diamond/copper composites and observed that thermal conductivity decreased with increasing carbide layer thickness and porosity. Chen et al.[9] melted Cu–X alloys (X = 1Co, 0.3B, 0.4Cr, and 1Ti wt%) under vacuum and demonstrated that Cu–matrix composites with interfacial layers exhibited enhanced interfacial bonding and higher thermal conductivity compared to pure Cu–matrix composites. Wei et al.[10] investigated Ti-modified diamond/copper composites by adding Ti to the Cu matrix or coating diamond particles with Ti. Wang et al.[11] applied magnetron sputtering to deposit Zr coatings (47–430 nm thick) on diamond surfaces, revealing that Zr coatings strengthened interfacial bonding and improved composite thermal conductivity. Although experimental approaches provide direct macro-performance data, they involve long cycles and high trial-and-error costs and struggle to precisely resolve the mechanistic coupling effects of microstructural parameters (e.g., interfacial layer thickness and residual stress distribution) on thermo-mechanical properties. Chen et al.[12] systematically reviewed the theoretical calculations of the thermal conductivity of copper–diamond composites, clarifying the applicable scenarios, core assumptions, and limitations of mainstream models. Their work reveals the sources of discrepancy between theoretical and experimental values, thereby providing a critical theoretical foundation for predicting and optimizing the thermal performance of such materials.

In this study, first-principles calculations were employed to investigate three interfacial structures: copper/zirconium carbide (Cu/ZrC), copper/titanium carbide (Cu/TiC), and copper/tungsten carbide (Cu/WC), exploring their stronger binding ability. Utilizing COMSOL Multiphysics simulations, parametric modeling enables rapid quantification of independent and interactive effects of variables including the diamond volume fraction, the particle size, and the interfacial layer thickness. Cross-validation with experimental literature data confirmed that the finite element method effectively reduces trial-and-error costs and provides pre-research guidance for complex interface optimization.

2. First-principles calculations of interfacial structures

The interfacial structure calculations in this work were performed using the Vienna Ab initio Simulation Package (VASP).[13,14] The projector augmented wave (PAW) method[15,16] was employed to describe core–valence electron interactions, while the exchange–correlation functional between electrons was treated within the generalized gradient approximation (GGA) using the Perdew–Burke–Ernzerhof (PBE) functional.[17] A plane-wave kinetic energy cutoff of 520 eV was applied for the basis set. Total energy calculations were deemed converged when the energy change per atom fell below 1.0×10^{-5} eV per atom. Sampling of the Brillouin zone was performed using Monkhorst–Pack k-point grids, centered at the Γ-point. For structural optimizations of the Cu/C, Cu/WC, Cu/ZrC, and Cu/TiC interfaces, k-point meshes of $9 \times 9 \times 1$, $9 \times 9 \times 1$, $2 \times 2 \times 1$, and $4 \times 4 \times 1$ were selected, respectively. Atomic geometries were optimized using the conjugate gradient algorithm.[16] Optimization was considered complete when the magnitude of the Hellmann–Feynman forces acting on each atom was less than 0.02 eV $Å^{-1}$.

Synthetic diamond predominantly exposes (100) and (111) surfaces. Cu, ZrC, and TiC all exhibit cubic crystal symmetry with face-centered cubic (FCC) Bravais lattices, where the close-packed planes correspond to the (111) orientation. WC adopts a (0001) basal plane. To elucidate the interfacial properties, we constructed three distinct interface models: TiC(111)/Cu(111), ZrC(111)/Cu(111), and WC(0001)/Cu(111).

To ensure crystallographic fidelity, all unit cell models were subjected to structural optimization. Calculated lattice parameters were rigorously validated against published computational and experimental reference data, as listed in Table 1. As can be seen from Table 1, the maximum discrepancy between our computed lattice parameters and previous computational results is up to 1.9%, while the maximum discrepancy compared with experimental results is 0.6%. The excellent agreement confirms the accuracy required for subsequent simulations.

The number of surface atomic layers was determined by measuring interlayer spacings after structural relaxation. Taking TiC as an example, the surface atomic relaxation results are summarized in Table 2,

$$\Delta_{ij} = \frac{d_{ij} - d_{ij}^0}{d_{ij}^0} \times 100\% \quad (1)$$

where d_{ij}^0 denotes the interlayer spacing between atomic layers i and j in the unrelaxed surface structure and d_{ij} represents the

Table 1 Calculated lattice parameters of Cu, diamond, TiC, WC, and ZrC compared with the computational and experimental reference data

	Our calculated lattice parameters (Å)	Computational reference data (Å)	Experimental reference data (Å)
Cu	3.63	3.63[18]	3.62[19]
Diamond	3.56	3.57[20]	3.57[21]
TiC	4.34	4.33[22]	4.33[23]
ZrC	4.72	4.63[24]	4.69[25]
WC	2.92	2.92[26]	2.91[27]

Table 2 Surface atomic relaxation results of TiC

Interlayer	Slab thickness, n				
	3	5	7	9	11
$\Delta 12$	−9.7	−16.3	−16.8	−17.6	−18.3
$\Delta 23$	—	4.6	9.6	11.2	11.4
$\Delta 34$	—	—	−4.0	−4.8	−5.3
$\Delta 45$	—	—	—	1.3	0.8
$\Delta 56$	—	—	—	—	−0.6

corresponding spacing after structural relaxation. As evidenced in Table 2, atomic relaxation primarily occurs within the first four surface layers, with interlayer spacing variations progressively stabilizing at greater depths. Convergence is achieved when the atomic layer count $n \geq 9$, where spacing changes diminish below the computational threshold, indicating that the TiC (111) surface exhibits bulk-like characteristics. Balancing computational efficiency against accuracy requirements, we constructed the interfacial model using a 9-layer TiC slab with Ti atoms as the surface-terminating layer (Layer 1).

Utilizing the same methodology, the surface structures of Cu and diamond were determined to comprise five and six layers, respectively; similarly, ZrC and WC surfaces were established as seven-layer and nine-layer structures, terminating with metal atoms. Cu/M (M = diamond, ZrC and WC) interfacial structures were constructed by vertically stacking the corresponding slabs, with the initial interfacial separation set to 2.5 Å. As evident from Table 1, the lattice parameters of the individual unit cells are not comparable. Therefore, it was necessary to redefine the surface vectors u and v for each surface structure to achieve mutual lattice matching at the interface. Lattice vector reconstruction was performed using the vaspkit-804[25] functionality to ensure that the lattice mismatch at the interface was reduced to below 5%, thereby facilitating the formation of stable interfacial structures. The lattice matching degree was calculated according to the following equation:

$$\Delta = \left| \frac{a_1 - a_2}{a_2} \right| \qquad (2)$$

where Δ is the lattice mismatch and a_1 and a_2 are surface lattice constants of material 1 and material 2, respectively.

Fig. 1 illustrates the atomic configurations and overlap patterns at the unoptimized interfaces for the four models: diamond/Cu, WC/Cu, TiC/Cu, and ZrC/Cu, with the corresponding top-down views of the interfacial structures presented below.

Based on the universal binding energy relation (UBER) theory,[28] we systematically analyzed the correlation between the work of adhesion and the interface separation distance for the four interfacial configurations presented in Fig. 2.

As illustrated in the UBER curve, the work of adhesion exhibits a descending order across the interfaces: TiC/Cu (d = 2.2 Å) > ZrC/Cu (d = 2.4 Å) > WC/Cu (d = 2.4 Å) > diamond/Cu (d = 2.0 Å). The work of adhesion is calculated according to the following equation:[29]

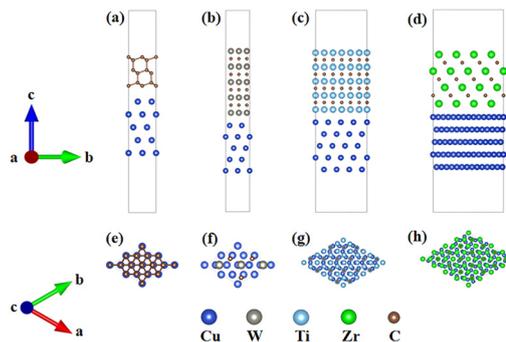$$W_{ad} = \frac{E_A^{slab} + E_B^{slab} - E_{A/B}}{S} \qquad (3)$$

Fig. 1 Four interfacial models (a) Diamond/Cu, (b) WC/Cu, (c) TiC/Cu, (d) ZrC/Cu; (e), (f), (g), and (h) show the corresponding top-down views.
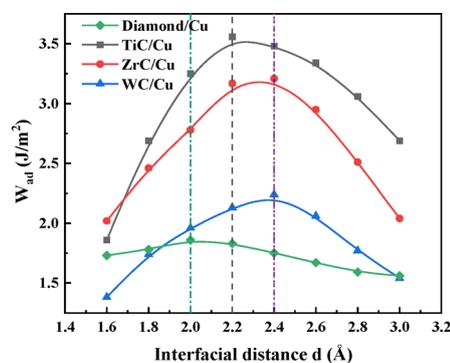

Fig. 2 UBER curves of work of adhesion and interface separation distance (d) for TiC/Cu, ZrC/Cu, WC/Cu, and diamond/Cu interface systems.

where $E_{A/B}$ is the total energy of the interface A/B, E_A^{slab} and E_B^{slab} represent the energies of the isolated surface slabs (of materials A and B, respectively) that constitute the interface A/B, and S denotes the interfacial area.

With non-interface atoms constrained, structural relaxation was performed on the interfacial configurations, followed by the calculation of the work of adhesion. The results are listed in Table 3. From the perspective of work of adhesion in Table 3, all three carbide/copper interfaces exhibit superior interfacial bonding compared to direct diamond/Cu bonding. This demonstrates that introducing carbide interlayers between Cu and diamond effectively enhances interfacial stability. Among the carbides, the TiC/Cu interface achieves the highest work of adhesion of 3.29 J m^{-2} (cf. ZrC/Cu: 2.94 J m^{-2}; WC/Cu: 2.57 J m^{-2}), indicating its optimal structural stability and bond strength. These results directly guide subsequent heat transfer simulations of finite element analysis.

3. Finite element results and discussion

3.1. Finite element computational model

COMSOL Multiphysics software has been widely used for analysis of the heat transfer process.[30] The steady-state simulation of the three-dimensional model was performed to analyze the thermal conductivity of the composite using the solid heat

Table 3 Equilibrium interface separation and work of adhesion for unrelaxed and fully relaxed configurations

	Unrelaxed		Fully relaxed	
Structure	Interface separation d/Å	Work of adhesion W_{ad}/(J m^{-2})	Interface separation d/Å	Work of adhesion W_{ad}/(J m^{-2})
Diamond/Cu	2.00	2.16	2.08	1.94
TiC/Cu	2.20	3.57	2.27	3.29
ZrC/Cu	2.40	3.21	2.29	2.94
WC/Cu	2.40	2.24	2.33	2.57

transfer module, along with its thermal expansion coefficient (CTE) using the solid mechanics module.

Fig. 3 shows a schematic diagram of the three-dimensional finite element model for the diamond/TiC/copper composite. The model features diamond particles, each surrounded by a titanium carbide (TiC) layer, embedded within copper matrix composites.

Without considering the actual microstructural details of the interface, an interfacial thermal conductivity model was theoretically established based on the acoustic mismatch model (AMM), a prevalent approach for analyzing interfacial thermal transport in diamond/Cu composites as discussed in prior reviews.[12] Subsequently, the interfacial thermal conductances of the diamond/TiC and TiC/Cu interfaces were calculated separately. The results of this work can lay a foundation for the subsequent import of interfacial thermal conductivity parameters into COMSOL software to perform simulations of the overall thermal conductivity. Specifically, the calculation method of interfacial thermal resistance based on the AMM is as follows:[31–33]

$$h = \frac{1}{4} \cdot \rho_m \cdot c_m \cdot \nu_m \cdot \eta \qquad (4)$$

where h is the interfacial thermal conductance (W m^{-2} K^{-1}), c_m is the specific heat capacity (J kg^{-1} K^{-1}), ρ_m is the density (m s^{-1}), ν_m is the Debye sound velocity (m s^{-1}), and η is the phonon transmission probability.

The coupling effects between electrons in metals and phonons in dielectrics at the interface do not contribute significantly to interfacial heat transfer. Thus, it can be assumed that heat conduction occurs primarily through phonon
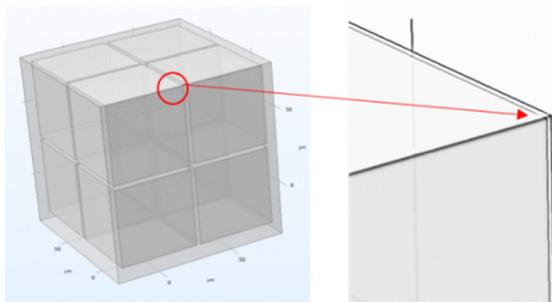
Fig. 3 Schematic diagram of the COMSOL model.

transmission. In this scenario, the phonon transmission probability η is expressed as follows:[31–33]

$$\eta = \frac{\rho_{in}\rho_{tran}\nu_{in}^3}{\nu_{tran}(\rho_{in}\nu_{in} + \rho_{tran}\nu_{tran})^2} \qquad (5)$$

where η is the phonon transmission probability, ρ_{in} is the emitter-side phonon density (kg m^{-3}), ρ_{tran} is the receiver-side phonon density (kg m^{-3}), ν_{in} is the emitter-side Debye sound velocity (m s^{-1}), and ν_{tran} is the receiver-side Debye sound velocity (m s^{-1}).

According to Debye thermal conductivity theory, the Debye sound velocity is calculated as follows:[31–33]

$$\nu = \left(\frac{3\nu_l^2\nu_t^2}{\nu_l^2 + \nu_t^2}\right)^{\frac{1}{2}} \qquad (6)$$

where ν is the Debye sound velocity of the medium (m s^{-1}), ν_l is the longitudinal sound velocity of the medium (m s^{-1}), and ν_t is the transverse sound velocity of the medium (m s^{-1}).

After calculating the total interfacial thermal resistance of the composite material, it is substituted into the thermal conductivity formula for diamond/copper composites to compute the theoretical thermal conductivity k_c of the Ti-coated diamond/copper composite material. The calculation of k_c is given by the following equation:[31–33]

$$\left(\frac{k_c - k_p^{eff}}{k_m - k_p^{eff}}\right) \cdot \left(\frac{k_m}{k_c}\right)^{\frac{1}{3}} = V_d \qquad (7)$$

$$k_p^{eff} = \frac{k_p}{1 + \frac{k_p}{h_d}} \qquad (8)$$

where k_c is the theoretical thermal conductivity of the Ti-coated diamond/copper composite (W m^{-1} K^{-1}), k_m is the thermal conductivity of the copper matrix (W m^{-1} K^{-1}), k_p is the thermal conductivity of the diamond reinforcement (W m^{-1} K^{-1}), and V_d is the volume fraction of diamond; d is the diamond particle size (μm), and h is the total interfacial thermal conductance of the Ti-coated diamond/copper composite (W m^{-2} K^{-1}).

Calculated results are shown in Table 4 The diamond/TiC interfacial thermal conductance is 2.67×10^8 W m^2 K, while that for the TiC/copper interface is 5.62×10^8 W m^2 K. However, practical composites often exhibit imperfect interfacial bonding and contain pores. To account for these effects, we introduce a correction factor δ applied to the interfacial thermal resistance, leading to the following expression for effective interfacial thermal conductance:

$$h_{eff} = 0.02h \qquad (9)$$

After correction, the diamond/TiC interfacial thermal conductance is 5.43×10^6 W m^2 K, and the TiC/Cu interfacial thermal conductance is 11.24×10^6 W m^2 K.

As shown in Fig. 4, in the boundary condition setting stage of the thermal conductivity simulation in COMSOL, by applying different temperature values to the two opposite surfaces, respectively, the simulation of unidirectional heat flow can be achieved. The magnitude of the temperature difference does not

Table 4 Fundamental parameters of TiC[34]

Materials	K (W m^{-1} K^{-1})	ρ (kg m^{-3})	c (J kg^{-1} K^{-1})	v_l ($\times$ 10^3 m s^{-1})	v_t ($\times$ 10^3 m s^{-1})
Cu	400	8960	385	4.91	2.5
Diamond	1800	3520	516	17.5	12.8
TiC	36.4	4930	568	10.37	6.47

affect the results. Adiabatic boundaries are applied to all remaining faces. Interfacial thermal resistance is one of the primary factors affecting the thermal conductivity of composites. Thermal contact resistance is introduced at the interfaces between diamond and the interlayer, and between the interlayer and Cu, to bring the simulation results closer to experimental values. Given that mesh fineness exerts a negligible influence on the model's simulation results, a conventional mesh element size, which is regulated by physics-controlled settings, suffices for the simulation.

Heat transfer is a steady-state process. Assuming constant power output from the heat source during operation, the thermal conductivity is determined using Fourier's law, as expressed in the following equation:[35]

$$\lambda = -\frac{q}{\dfrac{\partial T}{\partial x}} = -\frac{Q}{A\dfrac{\partial T}{\partial x}} \tag{10}$$

where Q is the total heat transfer (W), q is the heat flux (W m^{-2}), λ is the thermal conductivity (W m^{-1} K^{-1}), A is the cross-sectional area perpendicular to the heat flow direction (m^2), and $\partial T/\partial x$ is the temperature gradient (K m^{-1}).

For the thermal expansion coefficient simulation, the reference temperature is 20 °C, and the coefficient is evaluated over a temperature increase of 100 °C. Assuming an initial length L of the object before heating, the post-heating length increases by ΔL with a temperature change of ΔT. Adopting a conventional mesh fineness suffices for the simulation. The linear thermal expansion coefficient (α) is then calculated using the following equation:

$$\alpha = \frac{\Delta L}{L \cdot \Delta T} \tag{11}$$

3.2. Influence of the TiC layer thickness on thermal conductivity and the thermal expansion coefficient

For the finite element simulations, the following physical parameters were employed: diamond thermal conductivity: 1800 W m^{-1} K^{-1}; TiC thermal conductivity: 36.4 W m^{-1} K^{-1};
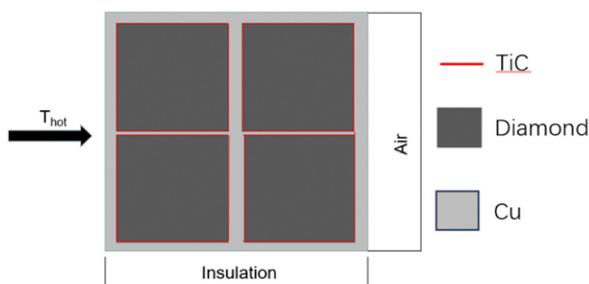
Cu thermal conductivity: 385 W m^{-1} K^{-1}; diamond particle size: 200 μm; and diamond volume fraction: 60 vol%.

Xiong[36] investigated diamond samples with a TiC interlayer thickness of 50 nm. The study by Xiong revealed that when preparing samples with thinner coatings *via* magnetron sputtering, plating voids occurred on partial diamond surfaces due to insufficient substrate rotation frequency. Consequently, this study excludes simulations for interlayers with a thickness of below 100 nm. Our simulation results align with the experimental trend reported by Xiong regarding the influence of the coating thickness on the thermal conductivity of Ti-coated diamond/CuCr composites (diamond size: 100 μm and volume fraction: 63 vol%) – specifically, thicker interlayers correspond to lower composite thermal conductivity. Therefore, a TiC interlayer thickness of 100 nm was selected for subsequent simulations. Simulations demonstrate a linear dependence of thermal conductivity on the TiC layer thickness. Fitting the simulation data and theoretical thermal conductivity yields the following expression:

$$y = 765 - 0.02x \tag{12}$$

The fitting equation for theoretical thermal conductivity is

$$y = 372 \cdot e^{-\frac{x}{357}} + 678 \tag{13}$$

where x is the TiC interlayer thickness (nm)

As shown in Fig. 5, the influence of the TiC interlayer thickness within the range of 100–500 nm on the thermal properties of the composite material presents distinct trends. The thermal conductivity, represented by the blue curve, decreases linearly. When the TiC interlayer thickness increases from 100 nm to 500 nm, the thermal conductivity drops from 959 W m^{-1} K^{-1} to 770 W m^{-1} K^{-1}, a reduction of 19.7%. In contrast, the decrease in the coefficient of thermal expansion (red curve) is relatively moderate, decreasing from 7.21 $\times$ 10^{-6}/K at a TiC interlayer thickness of 100 nm to 7.15 $\times$ 10^{-6}/K at

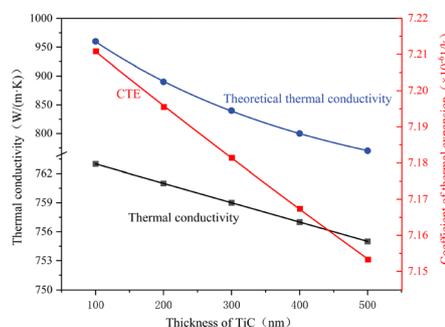**Fig. 4** Schematic diagram of the 2D physical field.

Fig. 5 Relationship between the TiC interlayer thickness and the thermal conductivity/thermal expansion coefficient.

500 nm. The results obtained from the AMM model (blue curve) are consistently higher than COMSOL simulation results (black curve, with values ranging approximately from 756 to 765 W m^{-1} K^{-1}). This discrepancy is attributed to the AMM model's insufficient consideration of interfacial thermal resistance constraints. Conversely, COMSOL simulations incorporate corrected interfacial thermal conductance parameters, which can better reflect complex interfacial effects such as pores and bonding imperfections, thus showing a closer match with experimental results and demonstrating superior predictive reliability. Therefore, the COMSOL-based numerical model with modified interfacial parameters can more accurately represent the true variation pattern of the composite material's thermal conductivity.

3.3. Influence of the diamond volume fraction on thermal conductivity and the thermal expansion coefficient

With the particle size of diamond (200 μm) and the thickness of the TiC layer (100 nm) fixed as constant parameters, the effects of the diamond volume fraction (10–70% vol%) on the thermal conductivity and coefficient of thermal expansion (CTE) of the composite were systematically investigated. To quantify the influence of the volume fraction, the diamond volume fraction was selected at an interval of 20 vol%, corresponding to the investigation points of 10%, 30%, 50%, and 70% vol%, respectively.

Our simulation results align with the experimental trends reported by Zhao *et al.*[37] who employed diamond particles of diameter 75–90 μm to fabricate diamond/copper composites at volume fractions of 50 vol%, 60 vol%, 70 vol%, and 80 vol% using both high-temperature high-pressure (HPHT) powder metallurgy and HPHT melt infiltration methods. Both sintering techniques demonstrated that thermal conductivity increased at volume fractions below 70 vol%, peaked at 70 vol%, and decreased at 80 vol%. This reduction occurs because higher diamond volume fractions shift load-bearing responsibility to diamond particles, inducing direct diamond–diamond contact after sintering. Simultaneously, finite copper melt inadequately fills interparticle gaps. During the pressure reduction and cooling stage, the already insufficient Cu melt solidifies and undergoes volumetric shrinkage, generating micro-voids at diamond/copper interfaces. Current simulations cannot comprehensively model these phenomena. Consequently, this study excludes simulations for diamond volume fractions exceeding 70 vol%. Fitting the simulation data and theoretical thermal conductivity yields the following expression:

$$y = 127\mathrm{e}^{-x/47} + 274 \qquad (14)$$

The fitting equation for theoretical thermal conductivity is

$$y = 321 + 11x \qquad (15)$$

where x is the diamond volume fraction (%).

As shown in Fig. 6, the red curve in the figure shows that the thermal expansion coefficient decreases nonlinearly from $18 \times 10^{-6}/°C$ (at 10 vol% diamond) to $6 \times 10^{-6}/°C$ (at 70 vol%). Meanwhile, the theoretical thermal conductivity (blue curve) increases significantly from 400 W m^{-1} K^{-1} to 1080 W m^{-1} K^{-1} over the same volume fraction range. However, the COMSOL-
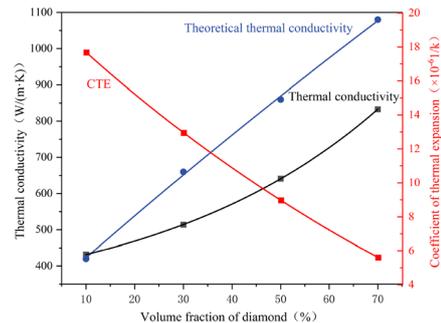

Fig. 6   Relationship between the diamond volume fraction and the thermal conductivity/thermal expansion coefficient.

calculated thermal conductivity (black curve), which accounts for interfacial thermal resistance and microstructural defects, remains consistently lower than the theoretical values, rising from 400 W m^{-1} K^{-1} to 800 W m^{-1} K^{-1}. This overestimation by the theoretical model primarily originates from inadequate consideration of interfacial phonon scattering and material heterogeneity. In contrast, COMSOL simulations incorporating modified interfacial thermal conductance parameters yield results that better align with the practical heat transfer behavior of composites.

3.4. Influence of the diamond particle size on thermal conductivity and the thermal expansion coefficient

To validate our simulation results, we referenced experimental parameters from the studies by Li[34] and Xiong:[36] diamond volume fraction ≈60 vol%. Combined with prior simulations on TiC interlayer thickness effects, fixed parameters of 60 vol% diamond fraction and 100 nm TiC thickness were used to evaluate the diamond particle size (50–300 μm).

Chen *et al.*[38] investigated diamond/copper composites with three diamond particle size ranges (50–60 μm, 180–212 μm, and 500–600 μm) using HPHT powder metallurgy and HPHT melt infiltration methods. Their results demonstrate that thermal conductivity increases with larger particle sizes. Furthermore, our simulation results align with experimental findings: Li *et al.*[34] achieved 752 W m^{-1} K^{-1} using 230 μm diamond particles with titanium additives; Xiong reported a maximum thermal conductivity of 654 W m^{-1} K^{-1} with 100 μm diamond particles at a 63 vol% fraction coated with 100 nm Ti. As confirmed by Chen *et al.*,[4] the composite reaches a peak thermal conductivity of approximately 704 W m^{-1} K^{-1} with a diamond size of 120 μm, a 50 vol% fraction, and a 400 nm TiC interfacial layer. This optimal experimental value matches the performance trend forecasted by our simulation. Fitting the simulation data and theoretical thermal conductivity yields the following expression:

$$y = -9628\mathrm{e}^{-x/8.37} \pm 306\mathrm{e}^{-x/172.98} + 835 \qquad (16)$$

The fitting equation for theoretical thermal conductivity is

$$y = -308 \times \exp(-x/325) + 1184 \qquad (17)$$

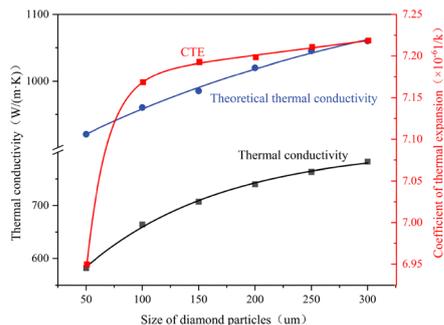where x is the diamond particle size (μm).

Fig. 7 Relationship between the diamond particle size and the thermal conductivity/thermal expansion coefficient.

As shown in Fig. 7, with the increase of the diamond particle size, the theoretical thermal conductivity (blue curve) rapidly rises as the diamond particle size increases, from approximately 920 W m^{-1} K^{-1} to 1060 W m^{-1} K^{-1}; the thermal conductivity simulated by COMSOL (black curve) also increases relatively slowly, but still shows an upward trend. The thermal expansion coefficient (red curve, CTE) also increases with the increase of the diamond particle size, approximately 6.95×10^{-6}/K when the particle size is 50 μm, and rises to approximately 7.25×10^{-6}/K when the particle size is 300 μm. The theoretical values exhibit systematic overestimation, particularly showing pronounced deviations from COMSOL-simulated thermal conductivity in the smaller particle size range. This discrepancy is attributed to the AMM model's assumption of ideal interfacial contact, which inadequately accounts for the constraining effects of interfacial thermal resistance (*e.g.*, phonon scattering and lattice mismatch) in practical materials. By incorporating modified interfacial thermal conductance parameters (such as interfacial thermal resistance and porosity distribution) in COMSOL, the calculated results demonstrate closer alignment with experimental observations.

4. Conclusions

This study systematically investigates interface optimization and thermal performance regulation mechanisms in diamond/copper composites through first-principles VASP calculations and COMSOL finite element simulations. First-principles computations identified titanium carbide (TiC) as the optimal interfacial layer, with the Cu/TiC interface exhibiting the highest adhesion work (3.29 J m^{-2}). Subsequent COMSOL simulations incorporating modified interfacial thermal conductance parameters yielded results that closely aligned with experimental data, while resolving the overestimation inherent in the acoustic mismatch model (AMM), thereby confirming the critical influence of interfacial effects on thermal conductivity and establishing a reliable predictive framework for thermal design. Parametric analysis revealed that both thermal conductivity and the coefficient of thermal expansion increase with increasing diamond particle sizes, with thermal conductivity stabilizing within the 150–200 μm range, recommending this cost-effective particle size. Conversely, thermal conductivity increases while the coefficient

of thermal expansion decreases with increasing diamond volume fractions, necessitating >45 vol% diamond to match the semiconductor coefficient of thermal expansion requirements ($4-9 \times 10^{-6}$ K^{-1}). Increasing the TiC interlayer thickness reduces both properties, though thermal conductivity exhibits greater sensitivity due to TiC's intrinsically low thermal conductivity, while the coefficient of thermal expansion reduction remains marginal owing to the interlayer's limited volumetric contribution. Notably, a limitation of this study is that it has not fully accounted for defects such as pores and interfacial voids in real composites. Collectively, this work provides computational guidance for experimental optimization of diamond-reinforced composites in electronic packaging.

Conflicts of interest

The authors declare that they have no known competing financial interest or personal relationships that could have appeared to influence the work reported in this study.

Data availability

The data supporting this article have been included as the first-principles calculations.zip and COMSOL simulations.zip.

Supplementary information (SI) is available. See DOI: https://doi.org/10.1039/d5ma01082a.

References

1 S. G. Dai, J. W. Li and C. J. Dong, Research Progress on Preparation Methods of High Thermal Conductivity Diamond/Copper Composites, *Fine Chem.*, 2019, **36**, 1995–2008.
2 C. Zweben, Advances in high-performance thermal management materials: a review, *J. Adv. Mater.*, 2007, **39**, 3–10.
3 L. F. Deng, X. K. Zhu and J. M. Tao, *et al.*, Application of Active Element to Cu/diamond Composites, *Electron. Process Technol.*, 2009, **30**, 128–132.
4 H. Chen, K. Chen, Y. Zhang, J. Li and X. Leng, Influence of Ti content on microstructure and thermal conductivity of diamond/Cu composites fabricated by spark plasma sintering, *Mater. Lett.*, 2026, **405**.
5 X. Z. Wu, D. Q. Wan and W. Zhang, *et al.*, Constructing efficient heat transfer channels at the interface of iamond/Cu composites, *Compos. Interfaces*, 2021, **28**, 625–635.
6 C. Zhang, R. C. Wang, Z. Y. Cai, C. Q. Peng, Y. Feng and L. Zhang, Effects of dual-layer coatings on microstructure and thermal conductivity of diamond/Cu composites prepared by vacuum hot pressing, *Surf. Coat. Technol.*, 2015, **277**, 299–307.
7 C. Y. Chung, M. T. Lee, M. Y. Tsai, C. H. Chu and S. J. Lin, High thermal conductive diamond/Cu–Ti composites fabricated by pressureless sintering technique, *Appl. Therm. Eng.*, 2014, **69**, 208–213.
8 Y. L. Wang, K. Y. Duan and K. K. Wang, *et al.*, Structure and thermal properties of layered Ti-clad iamond/Cu composites

prepared by SPS and HP, *Rare Met. Mater Eng.*, 2018, **47**, 2011–2016.

9   H. Chen, C. C. Jia, S. J. Li, X. Jia and X. Yang, Selective interfacial bonding and thermal conductivity of diamond/Cu-alloy composites prepared by HPHT technique, *Int. J. Miner., Metall. Mater.*, 2012, **19**, 364–371.

10 C. L. Wei, X. X. Wang, P. Tong, P. Wang and J. Wen, Effect of different titanium addition methods on the properties of diamond/Cu composites, *J. Mater. Res. Technol.*, 2024, **31**, 2014–2022.

11 L. H. Wang, Interfacial structure and thermal conductivity of Cw/diamond composites, Doctoral dissertation, University of Science and Technology Beijing, China, 2019.

12 K. Chen, X. S. Leng, R. Zhao, Y. Y. Kang and H. S. Chen, Progress in the Copper-Based Diamond Composites for Thermal Conductivity Applications, *Crystals*, 2023, **13**, 6.

13 G. Kresse and J. Furthmüller, Efficiency of ab-initio total energy calculations for metals and semiconductors using a plane-wave basis set, *Comput. Mater. Sci.*, 1996, **6**, 15–50.

14 G. Kresse and J. Hafner, Ab initio molecular-dynamics simulation of the liquid-metal–amorphous-semiconductor transition in germanium, *Phys. Rev. B: Condens. Matter Mater. Phys.*, 1994, **49**, 14251.

15 P. BLöChl, Projector augmented-wave method, *Phys. Rev. B: Condens. Matter Mater. Phys.*, 1994, **49**, 17953.

16 G. Kresse and D. Joubert, From ultrasoft pseudopotentials to the projector augmented-wave method, *Phys. Rev. B: Condens. Matter Mater. Phys.*, 1999, **59**, 1758.

17 J. R. Shewchuk, *An introduction to the conjugate gradient method without the agonizing pain*, Carnegie Mellon Univ., 1994.

18 X. Z. Pang, J. B. Yang, M. J. Pang, J. X. He, W. C. Yang, H. Q. Qin and Y. Z. Zhan, Theoretical Understanding of Atomic and Electronic Structures of the ZrC(111)/Cu(111) Interface, *J. Alloys Compd.*, 2019, **791**, 431–437.

19 Y. D. Zhu, M. F. Yan, Y. X. Zhang and C. S. Zhang, First-principles Investigation of Structural, Mechanical and Electronic Properties for Cu–Ti Intermetallics, *Comput. Mater. Sci.*, 2016, **123**, 70–78.

20 K. X. Gu, M. J. Pang and Y. Z. Zhan, Insight into interfacial structure and bonding nature of diamond (001)/Cr_3C_2 (001) interface, *J. Alloys Compd.*, 2019, **770**, 82–89.

21 P. D. Ownby, X. Yang and J. Liu, Calculated X-ray diffraction data for diamond polytypes, *J. Am. Ceram. Soc.*, 1992, **75**, 1876–1883.

22 S. L. Zhang, J. B. Wang and L. X. Rao, *et al.*, Electronic Characteristic, Tensile Cracking Behavior and Potential Energy Surface of TiC(111)/Ti(0001) Interface: A First Principles Study, *Chin. J. Aeronaut.*, 2023, **36**, 451–463.

23 A. Arya and E. A. Carter, Structure, Bonding, and Adhesion at the TiC(100)/Fe(110) Interface from First Principles, *J. Chem. Phys.*, 2003, **118**, 8982–8996.

24 R. O. Elliott and C. P. Kempter, Thermal expansion of some transition metal carbides, *J. Phys. Chem.*, 1958, **62**, 630–631.

25 X. H. Li, Y. Yan, J. H. Li, J. J. Gong, Y. X. Wang and Z. Chen, Effect of Alloying Elements on Interfacial Properties and Mechanical Behavior of Mg/WC Systems: A First-Principles Study, *Comput. Mater. Sci.*, 2024, **232**, 112630.

26 A. S. Kurlov and A. Gusev, Phase Equilibria in the W–C System and Tungsten Carbides, *Russ. Chem. Rev.*, 2006, **75**, 617–636.

27 V. Wang, N. Xu, J. C. Liu, G. Tang and W. T. Geng, VASPKIT: A User-Friendly Interface Facilitating High-Throughput Computing and Analysis Using VASP Code, *Comput. Phys. Commun.*, 2021, **267**, 108033.

28 J. H. Rose, J. Ferrante and J. R. Smith, Universal binding energy curves for metals and bimetallic interfaces, *Phys. Rev. Lett.*, 1981, **47**, 675.

29 W. Jin, L. Li, S. Zhang, H. Yang, K. Gao, X. Pang and A. A. Volinsky, *Chem. Phys. Lett.*, 2018, **713**, 153e159.

30 Y. L. Zhu, Y. H. Chen and L. Gou, The Improvement in Heat Transfer Performance of Single Crystal Silicon Carbide with Diamond Film, *J. Cryst. Growth*, 2024, **630**, 127601.

31 J. Molina, R. Prieto, J. Narciso and E. Louis, The effect of porosity on the thermal conductivity of Al–12wt.% Si/SiC composites, *Scr. Mater.*, 2009, **60**(7), 582–585.

32 Y. Zhang, H. L. Zhang, J. H. Wu and X. T. Wang, Enhanced thermal conductivity in copper matrix composites reinforced with titanium-coated diamond particles, *Scr. Mater.*, 2011, **65**(12), 1097–1100.

33 Z. Tan, Z. Li, D.-B. Xiong, G. Fan, G. Ji and D. Zhang, A predictive model for interfacial thermal conductance in surface metallized diamond aluminum matrix composites, *Mater. Des.*, 2014, **55**, 257–262.

34 J. W. Li, H. L. Zhang, L. H. Wang, Z. F. Che, Y. Zhang, J. G. Wang, M. J. Kim and X. T. Wang, Optimized Thermal Properties in Diamond Particles Reinforced Copper-Titanium Matrix Composites Produced by Gas Pressure Infiltration, *Composites, Part A*, 2016, **91**, 189–194.

35 A. Rape, K. Gott and A. Kulkarni, *et al.*, Simulation of matrix conductivity in copper–diamond composites sintered by field assisted sintering technology, *Comput. Mater. Sci.*, 2015, **110**, 29.

36 M. L. Xiong, Interface Microstructure and Thermal Properties of Titanium Coated Diamond/Copper Composites, Master's thesis, Harbin Institute of Technology, China, 2018.

37 L. Zhao, X. P. Song and Y. J. Zhang, *et al.*, Research on the preparation of diamond/copper composite materials by high temperature and high pressure method, *Diamond Abrasives Eng*, 2018, **38**, 15–19.

38 H. Chen, C. C. Jia, S. J. Li, X. Jia and X. Yang, Selective interfacial bonding and thermal conductivity of diamond/Cu-alloy composites prepared by HPHT technique, *Int. J. Miner., Metall. Mater.*, 2012, **19**, 364–371.